X-ray production in short laser pulse interaction with rare gas clusters

Emily Lamour, Christophe Prigent, Jean-Pierre Rozet, Dominique Vernhet

X-ray production in short laser pulse interaction with rare gas clusters

E Lamour, C Prigent, J P Rozet and D Vernhet

Institut des NanoSciences de Paris, CNRS UMR 75-88, Université Pierre et Marie Curie, Paris 6, 75015 Paris, France

Corresponding author's e-mail address: emily.lamour@insp.jussieu.fr

Abstract. Absolute keV x-ray measurements have been performed with nanometer size rare gas clusters submitted to femtosecond IR laser pulses at intensities I $<10^{17}$ W cm^{-2}. Special care has been taken in the measurements, by controlling the different parameters, which play a role in laser-cluster dynamics, *i.e.*, beam waist size, effective pulse length and energy profile of the laser, and the cluster size. In particular, the data obtained show evidence of low laser intensity threshold values for keV x-ray production, an optimum heating time when mapping the cluster dynamics by varying the pulse duration at constant laser energy and a saturation in the x-ray emission probability above a given cluster size.

1. Introduction

A fascinating feature of intense laser-matter interaction is its efficiency for converting photons in the eV range to x-rays with keV energies. It is now well known that large clusters, similarly to solids, couple very efficiently to intense subpicosecond laser pulses. Near 100 % of the laser radiation can be absorbed [1] leading to the observation of highly charged ions with energies reaching MeV [2], electrons with energies up to a few keV [3] and keV x-ray photons from inner-shell ionised atoms [4, 5, 6]. Most of the experimental results on kinetic energy distributions of ions or electrons [3, 7 and references therein] are quite well interpreted by either the nanoplasma model first introduced by Ditmire *et al* or microscopic calculations (see Ref [8] for a review of models). Whereas the spectroscopy of the emitted ions and electrons extracts information from the system a few microseconds after the femtosecond laser pulse and the cluster disintegration, x-ray spectroscopy allows performing measurements on a time scale down to a few tens of femtoseconds. Even though only ions with inner-shell vacancies contribute to x-ray spectroscopy, their observation gives access to the dynamical evolution of the irradiated cluster on a time scale comparable to that of the laser pulse duration. As an example, excited states of argon ions, from Ar^{12+} up to Ar^{16+}, with a K-shell vacancy are produced in laser heated clusters [5, 9, 10]: those states have lifetimes that can be as low as a few tens of femtoseconds (15 fs for the Ar^{16+} $^1P_1$ state). Since the inner-shell vacancies are produced by electron-impact ionisation, x-ray spectroscopy can provide deeper insight into the electron dynamics and more precisely on the heating mechanisms, which allow electrons to gain energy as high as the inner-shell binding energies. Only a few systematic experimental studies exist on the dependence with laser intensity, pulse length or cluster size [10, 11]. Some of them [10] have been qualitatively interpreted through the nanoplasma model which predicts a strong energy absorption at the resonance, *i.e.* when the plasma frequency in the cluster matches the laser frequency. This occurs during the

cluster expansion when a characteristic electron density is reached [12]. However, it has been argued [13] that this resonance should be strongly damped resulting in a large reduction of the electron temperatures. Recently, several microscopic approaches have been developed, based on Particle-In-Cell (PIC) methods [14], molecular dynamics [15] or Monte Carlo simulations [16] that take into account the non-isotropic and non-homogeneous character of the atomic and electronic distributions in the laser heated cluster. In this paper, we present experimental results that give extended clues on the nanoplasma dynamics, which aims to test these models.

KeV x-rays have been studied. They originate from rare-gas clusters irradiated with intense ($I < 10^{17}$ W cm^{-2}) infrared laser pulses of 50 – 800 fs duration. Argon and xenon clusters with more than 10^4 at./cl. (*i.e.* 10 - 40 nm of diameter) have been investigated. Measurements have been performed on the evolution of absolute photon yields and charge state distributions with different physical parameters governing the interaction; namely intensity, pulse duration of the laser as well as the size of the clusters. After a detailed description of the experimental conditions (section 2), we present a series of selected experimental results (section 3). We show the influence of the pulse length on the intensity threshold in the x-ray production and the evolution of the x-ray emission probability with the cluster size.

2. Experimental set-up and control of the physical parameters

Great care has been taken in the measurements by controlling the different parameters which play a role in the laser-cluster dynamics. Experiments have been performed on the LUCA facility (French acronym for Ultra Short Tunable Laser, CEA at Saclay) based on Chirp Pulse Amplification technique.

2.1. The laser

With a 20 Hz repetition rate, the facility delivers pulses centred at λ = 800 nm, of duration down to 50 fs after compression and of energy up to 100 mJ. An attenuator located behind the compressor system allows easily variations of the laser energy. The linearly polarized laser light with a diameter around 50 mm is focused by a 48 cm focal length lens placed in front of the entrance window of the main chamber (figure 1). The focal spot, imaged by a high sensitivity high dynamic camera, is found to be equal to 31 ± 1 µm in diameter at $1/e^2$ of the maximum laser intensity leading to an associated Rayleigh distance of 0.95 ± 0.1 mm and a nominal focal volume of $V_{nom.foc} = (7\pm1)\ 10^{-7}$ cm^3. An effective laser energy that contributes efficiently to the peak intensity can thus be determined and is found to be $\sim 45 \pm 5\%$ of the measured energy after the attenuator. We have checked that those properties do not depend on the incoming energy. The laser pulse duration is measured by a second order autocorrelator located after the compressor. Besides, to estimate the effective duration at the focal spot, spatio-temporal aberrations as the propagation time-delay and the group velocity dispersion mostly induced by the focusing lens have to be considered (effect of the entrance window being negligible). Bor and co-workers have developed a simple geometrical model [17], confirmed by experimental studies [18], to take into account these effects. Consequently, assuming a Gaussian pulse, we found an effective pulse duration of 59 fs at the focal point instead of 50 fs measured just after the compressor *i.e.* a broadening of 18%. The spatio-temporal aberrations decrease significantly when increasing the pulse duration giving rise to a broadening less than 1% for a 200 fs pulse. Control of these parameters allowed us to obtain laser intensities in the 10^{14} to 10^{17} W/cm² range determined with an accuracy better than $\pm$ 20%. Finally, the laser pulse temporal contrast measured by a third order autocorrelator is found to be much lower than 10^{-4} of the main pulse over an interval of 4 ps (further, the contrast falls down to 10^{-6}). No pre-pulse is observed avoiding a pre-ionisation of clusters and providing experimental conditions as clean as possible. In the following, only effective values will be given.

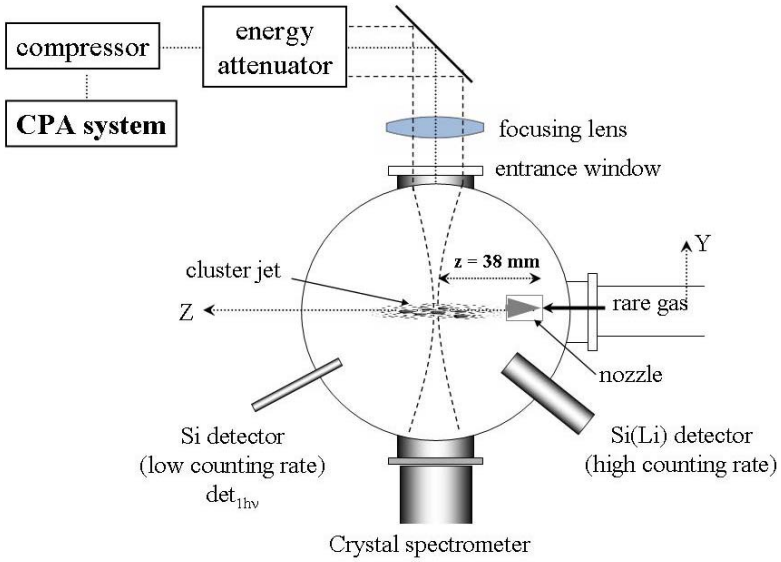

Figure 1. Schematic drawing of the main chamber of the experimental set up.

2.2. The cluster jet

For the cluster production, we make use of the condensation ability of a gas flow at high pressure (P_0) through a conical nozzle [19]. This nozzle is mounted on a solenoid pulsed valve operated at a repetition rate in the 1 - 20 Hz range. An opening duration of 500 µs insures to reach a stationary regime for the cluster formation [20].

The nozzle has a diameter (d) of either 300 or 1000 µm with a half opening angle (α) of 7.5° and a length (L) of 25 mm. In this paper, only results at a working distance z of 38 mm are presented (figure 1); z being the distance between the entrance of the conical nozzle and the interaction zone. Under such conditions, mean atomic densities of the order of 10^{17} at/cm^3 are obtained – these values have been checked recently through an electron impact technique.

To estimate the mean cluster size, several scaling laws [21] are applied, all based on the Hagena parameter [22]. A Compilation of the most recent cluster size measurements obtained by different experimental methods can be done and gives rise to the following law

$$< N >= 100 \cdot \left(\frac{A \times P_0(\text{bar}) \times d(\mu\text{m})^{0.85}}{1000} \right)^{1.8} \qquad (1)$$

where A = 15.36 for argon and 51.20 for xenon, under the conditions of the present experiments. Thus, cluster sizes range from a few 10^3 to 10^6 atoms/cluster. Controversial discussions on the clustering rate in the jet remain, and here, we just assumed a clustering rate of 100 %, which leads to a distance of 0.5 and 2 µm between clusters. As an example, at z = 38 mm and for a nozzle diameter of 300 µm, a xenon pressure of 10 bar corresponds to a mean atomic density of 7×10^{16} at/cm^3, a cluster size of 2×10^5 at/cl (*i.e.*, a diameter of 292 Å), a distance between clusters of 1.4 µm and consequently a number of clusters in the nominal focal volume of 2.6×10^5 clusters.

2.3. The detection system

The detection system has previously been described [4, 5]. Briefly, the isotropic [4] x-ray emission is analyzed by two semiconductor detectors and a high resolution high transmission Bragg-crystal spectrometer. These detectors are calibrated in efficiency and energy using standard x-ray sources and x-ray fluorescence of solid targets exposed to electron impact.

One of the semiconductor detectors ($det_{1h\nu}$) is specially designed to record single photon spectra (<< 1 hν / pulse) where the signal is then simply proportional to the photon energy. The other is suited to record moderate to high counting rates (~ 1 hν / pulse or >> 1 hν / pulse), taking advantage of the pileup mode. It allows to extract the number of photons simultaneously emitted since photon energy is determined for each recorded spectrum by $det_{1h\nu}$ [4, 5]. The combination of these two solid-state detectors allows us to observe the evolution of absolute x-ray yields over at least 4 orders of magnitude with uncertainties lower than 30 %. Up to 2×10^9 photons of around 3 keV (for argon clusters) per laser shot emitted in 4π have been measured.

State resolved measurements are performed using a crystal spectrometer equipped with a flat mosaic graphite crystal (HOPG) and a large (60×60 mm^2) home-made position sensitive detector working in the photon counting mode. Typical efficiency of around a few 10^{-6} can be reached. The following transitions are observed:

- Typical K x-rays characteristic of the $2p \rightarrow 1s$ deexcitation from Ar^{12+} to Ar^{16+} ions (Figure 2 and Ref [5]); a resolution of 1.7 eV at 3 keV allows observing the fine structure component of Ar^{16+} ($^1P_1$ and $^3P_1$);
- Typical L x-rays characteristics of the $3d_{3/2} \rightarrow 2p_{1/2}$ and $3d_{5/2} \rightarrow 2p_{3/2}$ deexcitations from Xe^{q+} ($q \geq 24$) with a 4 eV resolution at 4.4 keV [23].

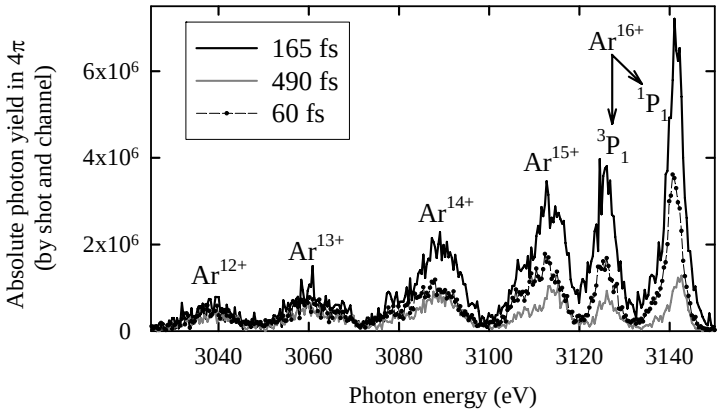

Figure 2. $1s2p n\ell \rightarrow 1s^2 n\ell$ high-resolution spectra recorded during irradiation of argon clusters by 800 nm and 9 mJ pulses for three different pulse durations, with $\langle N \rangle \sim 1.1\times10^6$ atoms/cluster (obtained with a nozzle diameter of d = 1 mm).

The whole of the spectrometers is then very well suited to follow the evolution of x-ray yields and the ionic distributions as a function of a given experimental parameter when controlling the others.

2.4. Spatial overlap between laser and clusters

Several degrees of freedom in our experimental system allow optimising the spatial overlap between the laser and the cluster jet. First, the delay (t_{VL}) between the opening of the valve and the incoming laser pulse can be varied so as to scan the cluster jet in the cluster propagation direction (Z). Second, the valve can be translated in the perpendicular direction (XY) to the cluster propagation axis to adjust the position of the incoming clusters with respect to the laser focal spot. Finally, the translation of the focusing lens along the laser propagation axis allows to optimise the position of the focal spot in the cluster jet. Typical yield measurements are displayed in figures 3 and 4 for both types of clusters (Ar

and Xe) and the optimum is found to be independent on the backing pressure *i.e.*, the cluster size and the mean atomic density. Indeed the mean atomic density remains low enough to prevent any problem of laser propagation (the laser focus is not modified) contrary to what may occur when using an ultra dense cluster jet [24]. The adjustments insure reproducible experimental conditions shot by shot (one laser shot for one cluster bunch). All of our experimental data are obtained at optimized overlap (arrows on figures 3 and 4).

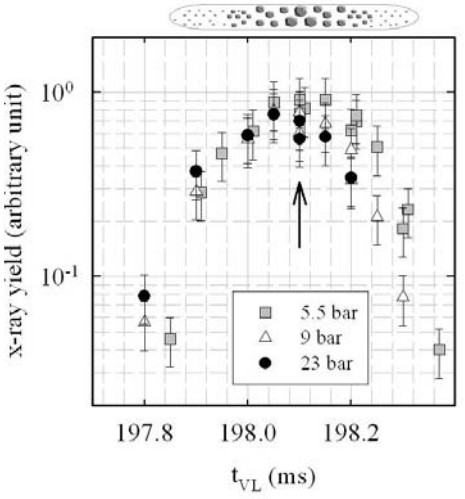

Figure 3. Normalised x-ray yield versus the delay between the opening of the valve and the laser pulse for three different xenon backing pressures. Top: sketch of the cluster bunch.

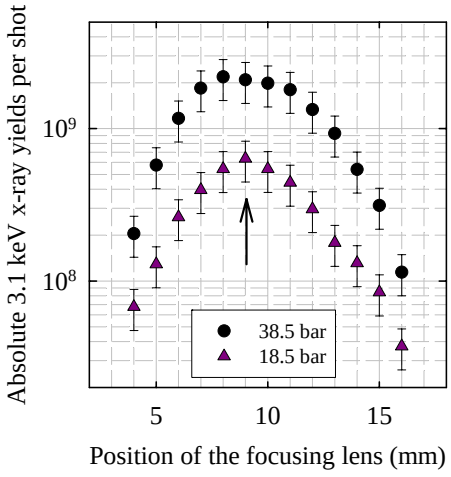

Figure 4. Absolute 3.1 keV x-ray yield measurements versus the position of the focusing lens for two different argon backing pressures.

3. Results and comments

3.1. Intensity threshold in the x-ray production

Figure 5 presents the x-ray yield (N_x) dependence with the laser peak intensity, I_{peak}, for xenon clusters and for two different effective laser pulse lengths (τ = 60 and 320 fs). Those results have been obtained by tuning only the laser energy. Whatever the cluster species, the cluster size, the mean atomic density, the laser wavelength and the pulse duration, clearly two regimes occur: a rapid increase after a well defined threshold (I_{th}) followed by a smooth evolution. Above the threshold, the evolution of the x-ray yield with the laser intensity can be accurately fitted, over 5 orders of magnitude, by the evolution of the effective focal volume $V_{eff.foc}$ given by [25]:

$$V_{eff.foc.} = V_{nom.foc.}\left\{\frac{4}{3}\cdot\left(\frac{I_{peak}}{I_{th}}-1\right)^{1/2}+\frac{2}{9}\cdot\left(\frac{I_{peak}}{I_{th}}-1\right)^{3/2}-\frac{4}{3}\cdot\mathrm{arctg}\left(\frac{I_{peak}}{I_{th}}-1\right)^{1/2}\right\}. \qquad (2)$$

In other words, the physical signal grows with the number of partners contained in this volume once the threshold value I_{th} has been reached: $N_x \propto V_{eff.foc}$. This suggests that the x-ray emission probability per atom, given by

$$P_{x-ray/at} = \frac{N_x}{< n >_{eff}} \qquad (3)$$

is constant (or almost constant) when $I_{peak} > I_{th}$ ($<n>_{eff}$, being the average number of atoms in the effective focal volume with $<n>_{eff} = \rho\ (at/cm^3) \times V_{eff.foc}$). In addition, one can deduce that ionisation probabilities of the L as well as the K-shells reach a saturation regime for a laser intensity around three times I_{th} since the mean charge state is found to be invariant [5].

As shown in figure 5, at 60 fs, the intensity threshold for the production of characteristic L x-rays lies at $I_{th} = 3.5\times10^{15}$ W/cm², which corresponds to a ponderomotive energy (*i.e.*, a maximum oscillation energy for free electrons in the laser field) of 420 eV, far too low to explain the creation of L-shell vacancies in xenon by electron impact (L binding energy ~ 4.2 keV). The same behavior has been already found for the production of K x-rays in the case of argon clusters [9, 16]. Beyond, the most striking feature is the strong dependence of this intensity threshold with the pulse length τ. As shown in figure 6 and despite the small number of values obtained so far, one can tentatively derive a fit function (dashed line),

$$I_{th}(\tau) = I_0 + A\exp(-B\times\tau) \qquad (4)$$

where A and B are two empirical parameters. One should note that I_0 is found close to the intensity threshold of Ar^{1+} or Xe^{2+} production by Optical Field Ionisation (OFI) *i.e.* ~ 2×10^{14} Wcm^{-2}, which corresponds to a ponderomotive energy of 30 eV!. Consequently, at such low laser intensities, the heating mechanisms involved seem to be efficient enough to accelerate electrons up to keV energies to produce inner-shell vacancies by electron impact.

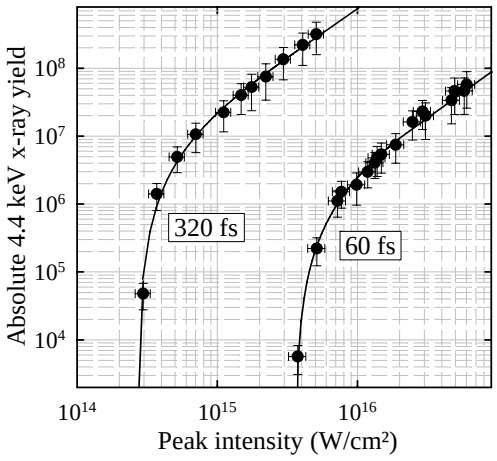

Figure 5. Absolute x-ray yield versus the laser intensity for 9 bar (1.7 10^5 at/cl) xenon clusters obtained for two different pulse durations. Solid lines are the normalized effective focal volumes with the experimental intensity thresholds (I_{th}): 3.5 10^{15} W/cm² for 60 fs and 2.5 10^{14} W/cm² for 320 fs.

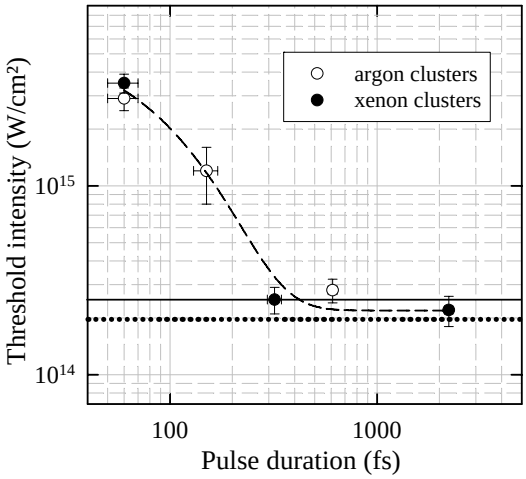

Figure 6. Intensity thresholds for the x-ray production versus the pulse duration for argon and xenon clusters. Dashed line: fit with a decay function (see text), horizontal solid line: the OFI threshold for producing Ar^{1+}, dotted line: the OFI threshold for producing Xe^{2+} (see text).

Recently, through a mean-field classical transport simulation, several effects have been investigated, such as the collective electron motion, electron-impact ionisation, cluster charging and elastic electron backscattering at the core potential of cluster ions in the presence of the laser field. Even if there is still discrepancy in the ionic charge state distribution, the evolution of the x-ray yield has been successfully reproduced for a pulse duration around 50-60 fs at laser intensities in the 10^{15} – 10^{16} W/cm² range [16].

3.2. Pulse duration dependence on the x-ray yield

Figure 2 shows ionic distributions for three pulse durations. Clearly, we observe an optimal pulse duration for total x-ray yield as well as for the highest charged states production. The pulse duration effect in the x-ray yield production is shown in figure 7 for the same large argon clusters. The laser fluence (2.4×10^3 J/cm²) is kept constant while the peak intensity decreases from 4×10^{16} (at 60 fs) to 3×10^{15} W/cm² (at 720 fs). The plot exhibits a maximum in the x-ray production for an optimal pulse duration of around 150 fs. No dependence with the cluster size is found within the examined cluster size range (radius from 170 to 250 Å [11]) contrary to previous studies performed with slightly larger

clusters in ultra dense jets [10]. Results in Ref [10] are qualitatively interpreted within the well-known nanoplasma model in which an optimal duration is expected when the resonance occurs at the maximum of the laser absorption but where no influence of the effective focal volume is considered. Here, applying the direct relation found between the effective focal volume and the absolute x-ray yield (section 3.1), one can derive its evolution with pulse duration using the fit function of I_{th} obtained experimentally (Eq.4). As illustrated in figure 8, the general trend is well reproduced apart from the exact position of the optimum. This demonstrates once more the influence of the effective focal volume even if other dynamical effects have to be considered such as cluster expansion which reduces the x-ray production and may shift the maximum towards lower pulse durations.

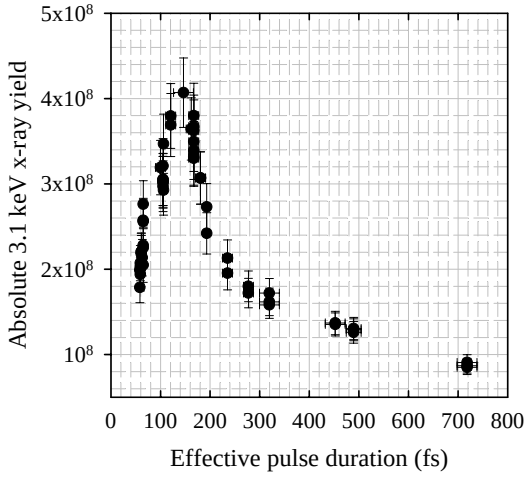

Figure 7. Evolution of the absolute x-ray yield with the effective pulse duration (τ) at constant energy (9 mJ) in the case of argon clusters with P_0 = 30 bar *i.e.* 1.1×10^6 at/cluster (radius 210Å)

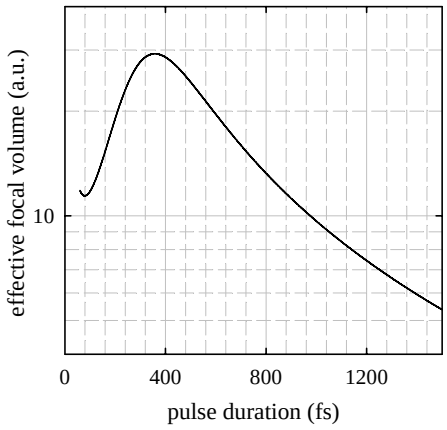

Figure 8. Evolution of the effective focal volume (Eq(2)) with the pulse duration taking into account the evolution of the intensity threshold with the pulse duration via Eq(4).

3.3. Cluster size dependence

As presented in section 2.2, the cluster size is tuned by changing the backing pressure P_0 as given by Eq (1). Nevertheless, changing P_0 modifies also the mean atomic density ρ, and to give a pertinent insight on the cluster size dependence, we choose to present the evolution of the x-ray emission probability per atom given by Eq (3). We assume that the effective focal volume does not vary with the cluster size over the whole range examined since roughly the same I_{th} value has been found for several different cluster sizes. A typical behaviour observed is illustrated in figure 9 for argon clusters submitted to 70 fs pulses with a peak intensity of 3.4×10^{16} W/cm² resulting in $V_{eff.foc.} \sim 6\times10^{-6}$ cm^3 with I_{th} around 2×10^{15} W/cm². A strong increase in the probability from 10^{-6} to 3.5×10^{-5} is observed, followed by a saturation for a cluster-size larger than 5×10^5 at/cl. It is worthwhile mentioning that, in the saturation region, the charge state distribution has still significant variation with cluster size, as presented in figure 9, showing evidence of an increase of the L shell ionisation. The same behaviour is observed with xenon clusters exhibiting even a stronger rise of the probability, from 2×10^{-7} to 2.5×10^{-5} (for respective cluster sizes, 5×10^4 and 2×10^6 at./cl. and nearly equivalent laser conditions). Here again, this result demonstrates a "simple" dependence of the x-ray yield as a function of the number of atoms in the effective focal volume, since $N_x = \rho \times V_{eff.foc} \times P_{x-ray/at}$ and ρ is proportional to P_0.

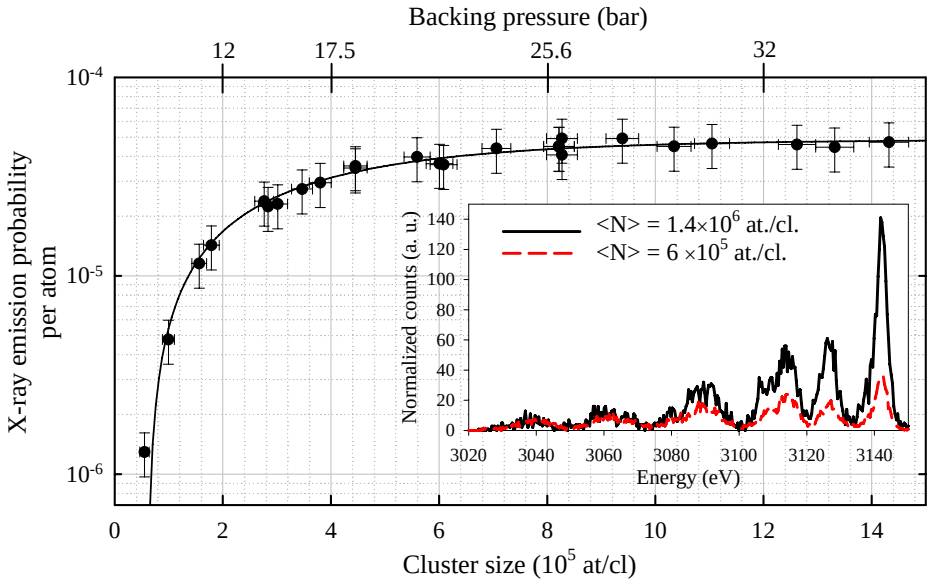

Figure 9. Evolution of the x-ray emission probability with argon cluster size at a peak intensity of 3.4×10^{16} W/cm² and a pulse length of 70 fs. Corresponding backing pressures are given on the top axis. The solid line is an eye-guiding line. The inset gives charge state distributions for 2 cluster sizes in the saturation regime: dashed line : <N> ~ 6×10^5 at/cl – solid line : <N> ~ 1.4×10^6 at/cl.

4. Conclusion

Absolute keV x-ray measurements have been performed on large rare gas clusters submitted to femtosecond laser pulses at moderate intensities (from 10^{14} to 10^{17} W/cm²). To obtain relevant results on plasma dynamics and electron heating processes, the effective energy and pulse duration in the focal spot have been carefully determined. Data reproducibility is insured by controlling the spatial overlap between the laser pulse and the cluster bunch, shot by shot. Under such conditions, we clearly demonstrate the x-ray probability to be constant (or almost constant) above a given laser intensity threshold and to saturate as well above a given cluster size. Both findings give clues for an x-ray yield simply driven by the number of atoms inside the effective focal volume once an intensity threshold is reached. In addition, our results indicate a strong pulse-duration dependence of the x-ray yield, which goes through an optimum that is directly connected to the intensity threshold evolution with the pulse duration. The production of inner-shell vacancies being very sensitive to energetic electrons produced during the interaction, the local cold plasma approximation used in the nanoplasma model is no longer valid. Analysis of the evolution of the high-energy part of the kinetic energy distribution of electrons as a function of pulse duration and cluster size is in progress using microscopic calculations [26].

[1] Krainov V P and Smirnov M B 2002 *Phys. Rep.* **370** 237
[2] Ditmire T, Tisch J W G, Springate E, Mason M B, Hay N, Smith R A, Marangos J and Hutchinson M H R 1997 *Nature* **386** 54
[3] Springate E, Aseyev S A, Zamith S and Vrakking M J J 2003 *Phys. Rev. A* **68** 053201
[4] Dobosz S, Lezius M, Schmidt M, Meynadier P, Perdrix M, Normand D, Rozet J P and Vernhet D 1997 *Phys. Rev. A* **56** R2526
[5] Rozet J P, Cornille M, Dobosz S, Dubau J, Gauthier J C, Jacquemot S, Lamour E, Lezius M, Normand D, Schmidt M and Vernhet D 2001 *Physica Scripta* **T92** 113
[6] Kumarappan V, Krishnamurthy M, Mathur D and Tribedi L C 2001 *Phys. Rev. A* **63** 023203
[7] Krishnamurthy M, Jha J, Mathur D, Jungreuthmayer Ch, Ramunno L, Zanghellini J and Brabec T 2006 *J. Phys. B: At. Mol. Opt. Phys.* **39** 625

[8] Saalmann U, Siedschlag Ch and Rost J M 2006 *J. Phys. B* **39** R39
[9] Lamour E, Dreuil S, Gauthier J C, Gobert O, Meynadier P, Normand D, Perdrix M, Prigent C, Ramillon J M, Rozet J P and Vernhet D, 2002 *Applications of X Rays Generated from Lasers and Other Bright Sources II, Proc. SPIE*, Eds G.A.Kyrala and J.C. Gauthier **4506** 97
[10] Dorchies F, Caillaud T, Blasco F, Bonté C, Jouin H, Micheau S, Pons B and Stevefelt J 2005 *Phys. Rev. E* **71** 066410
[11] Lamour E, Prigent C, Rozet J P and Vernhet D 2005. *NIM B* **235** 408
[12] Ditmire T, Springate E, Tisch J W G, Shao Y L, Mason M B, Hay N, Marangos J P and Hutchinson M H R 1998 *Phys. Rev.* A **57** 369; Milchberg H M, McNaught S J and Parra E 2001 *Phys. Rev.* E **64** 056402
[13] Megi F, Belkacem M, Bouchene M A, Suraud E, and Zwicknagel G 2003 *J. Phys. B* **36**, 273.
[14] Fukuda Y, Kishimoto Y, Masaki T and Yamakawa K 2006 *Phys. Rev. A* **73** 031201(R); Gupta A, Antonsen T M, Taguchi T and Palastro J 2006 *Phys. Rev. E* **74** 046408
[15] Last I, Jortner J 2007 *Phys. Rev. A* **75** 042507
[16] Deiss C, Rohringer N, Burgdörfer J, Lamour E, Prigent C, Rozet J P and Vernhet D 2006 *Phys. Rev. Lett.* **96** 013203
[17] Bor Z 1988 *J. Mod. Opt.* **35** 1907; Bor Z and Horvath Z L 1992 *Optics Communications* **94** 249
[18] Planchon T 2003 *PhD thesis* http://tel.archives-ouvertes.fr/tel-00005388
[19] Hagena O F and Obert W 1972 *J. Chem. Phys.* **56** 1793; Hagena O F 1987 *Z. Phys. D : Atoms, Molecules and Clusters* **4** 291
[20] Saenger K L and Fenn J B 1983 *J. Chem. Phys.* **79** 6043
[21] Wörmer J, Guzielsk Vi, Stapelfeldt J *et al* 1990 *Physica Scripta* **41** 490; Hagena O F 1992 *Rev. Sci. Ins.* **63** 2374; Buck U and Krohne R 1996 *J. Chem. Phys.* **105** 5408
[22] Hagena O F 1974 *The Physics of Fluids* **17** 894
[23] Adoui L, Gobert O, Indelicato P, Lamour E, Meynadier P, Normand D, Perdrix M, Prigent C, Rozet J P and Vernhet D 2003 *Nucl. Instr. and Meth. B* **205** 341
[24] Caillaud T, Blasco F, Bonté C, Dorchies F and Mora P 2006 *Phys. of Plasmas* **13** 033105
[25] Augst S, Meyerhofer D, Strickland D and Chin S L 1991 *J. Opt. Soc. Am. B* **8** 858
[26] Deiss *et al*, in these conference proceedings of ICPEAC-2007